# Trajectory Planning of Jumping over Obstacles for Hopping Robot

**Zhaohong Xu**
zhaohongxu@sjtu.edu.cn
Shanghai Jiao Tong University
School of Mechanical Engineering
200240 Shanghai, China

**Tiansheng Lü**
tslu@sjtu.edu.cn

**Fang Ling**
Shanghai Jiao Tong University
Engineering Training Center
200240 Shanghai, China

*Trajectory planning strategy is proposed to jump over an obstacle integrated three various dynamics in one-legged multi-joint hopping robot. A concept of inertia matching ellipsoid and directional manipulability are extended to optimize take-off postures. Optimized results have been used to plan hopping trajectory. Aimed at the sensitivity of motion trajectory to constraint conditions, a 6th polynomial function is proposed to plan hopping motion and it has a better robustness to the parameters change of constraint conditions than traditional 5th polynomial function. During flight phase, an iterative method and angular momentum theory are used to control posture to a desired configuration. In order to lift foot over an obstacle, correction functions are constructed under unchanged boundary constraint conditions. During stance phase, robot trajectories are planned based on internal motion dynamics and steady-state consecutive hopping motion principle. A prototype model is designed, and the effectiveness of the proposed method is confirmed via simulations and experiments.*
***Keywords**: multi-joint hopping robot, trajectory planning, inertia matching ellipsoid, iterative method*

## Introduction

Legged robots have better versatility, mobility and autonomous capability on uneven or discontinuous environment among mobile robotics family. One of the motivations to study one-legged robots is to gain a good understanding of system dynamics and extend it to human and animal locomotion. Multi-legged robot has some gaits, namely walking, hopping and running. However one-legged robot has only one gait, viz hopping.

Despite a great potential of hopping machines, their control and trajectory planning are still issues. Li and Montgomery (1990) proposed a closed-loop strategy that could optimally control body orientation of a one-legged robot during flight phase using the internal motion of the leg. They didn't use angular momentum to control body attitude in the whole hopping process. Ohashi and Ohnishi (2006) proposed a method of controlling the hopping height by changing the leg length at bottom taking account of torque limits of motors and described a way to estimate the actual thrust force. Babic and Omrcen (2006) performed vertical jump simulations using three different control algorithms including ZMP constraints. Although they described some valid method to control jumping height, take-off phase should not be ignored. De Man et al. (1998) developed a control algorithm for a one-legged hopping robot with an articulated leg. Similarly, Vermeulen (2003) developed a real-time applicable control algorithm for a planar one-legged robot on an irregular terrain based on the choice of objective locomotion parameters. Choosing appropriate parameters in real-time is complicated. The concept of kinematic manipulability ellipsoids was introduced by Yoshikawa (1985a and 1985b) as a measure of the capability of a manipulator for executing a specific task in a given configuration. A number of interesting extensions and applications of manipulability ellipsoids had appeared in robotic conceptual design and optimization during the last few years (Bowing and Khatib, 2005 and Kurazume and Hasegawa, 2006). Although some manipulability ellipsoids have been applied to redundant manipulators, there are some unsolved problems of trajectory planning in robotics.

This paper will study a trajectory planning of jumping over obstacles for a one-legged multi-jointed active hopping robot. The initial constraint conditions are obtained and optimized with inertia matching and directional manipulability. A 6th order polynomial function is constructed to track joint angle trajectory, its highest power coefficient is obtained with joint workspace constraints, and the others are determined with the initial and ultimate constraint conditions. This method has a better robustness to the parameters change of constraint conditions than the traditional 5th polynomial function. In order to control the robot posture to a desired configuration, an iterative method and angular momentum theory are applied.

## Nomenclature

*ZMP* =*Zero Moment Point*
*COG* =*Center of Gravity*
*IME* =*Inertia Matching Ellipsoid*
*SVD* = *Singular Value Decomposition*
*DOF* =*Degree of Freedom*
*F* = *flight phase*
*F* = *foot*
*S* = *stance phase*
*To* = *Take off*
*Td* = *Touch down*
*+* = *function evaluated after impact*
*-* = *function evaluated before impact*
*so* = *initial state during stance phase*
*sd* = *ultimate state during stance phase*

## Inertia Matching and Take-off Posture Optimization

The concept of inertia matching (Chen and Tsai, 1991) is widely used in the analysis of actuator and gear systems, primarily for selection of the optimum gear ratio based on the transmission performance between the torque produced at the actuator and the torque applied to the load. The proposed inertia matching ellipsoid characterizes the dynamic torque/force transmission efficiency between joint actuators and a load held by the end-effector of a manipulator. Inertia matching for hopping robot will be proposed in this paper as a new index of the dynamic performance.

Hopping process can be divided into three phases based on constrain conditions, viz stance phase, flight phase, and landing impact phase. Figure 1 depicts the hopping robot geometry which is a multi-body system in sagittal plane. It consists of four segments, a massless foot, a lower leg, an upper leg and body. Each joint (ankle, knee and hip) is driven by an actuator. Being a massless foot, it is considered as a point during flight.

**Paper accepted June, 2008. Technical Editor: Glauco A. de P. Caurin.**

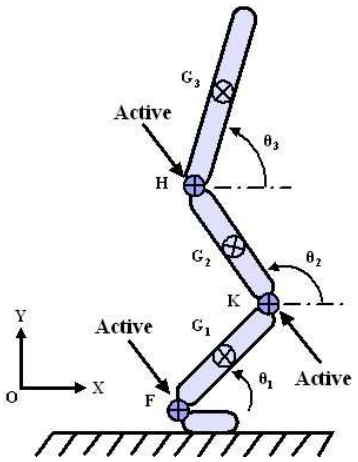


**Figure 1. One-legged multi-jointed active hopping robot.**

The mass of the i-th rigid body is $m_i$, its length is $l_i$, and the moment of inertia around its center of mass $G_i$ is $I_i$. The absolute angle between the horizontal axis and the i-th segment is $\theta_i$, the direction of anticlockwise is positive. The location of the center of mass $G_i$ of the leg is given by $\overline{\mathbf{FG}_1}=\alpha_1 l_1$, $\overline{\mathbf{KG}_2}=\alpha_2 l_2$ and $\overline{\mathbf{HG}_3}=\alpha_3 l_3$, where $0<\alpha_i<1$. The coordinates $\boldsymbol{\theta}$ are the absolute angles $(\theta_1,\theta_2,\theta_3)^T$, which describe the absolute shape of the robot. The robot's absolute position vector of COG $\mathbf{R}_G$ is specified by the Cartesian coordinates $(X_G,Y_G)^T$. The absolute position vector of foot $\mathbf{R}_F$ is specified by the Cartesian coordinates $(X_F,Y_F)^T$. During flight phase the vector of generalized coordinates $\mathbf{q}_f$ can be denoted as $(\theta_1,\theta_2,\theta_3,X_F,Y_F)^T$, and during stance phase the vector of generalized coordinates $\mathbf{q}_s$ can be denoted as $(\theta_1,\theta_2,\theta_3)^T$.

The concept of inertia matching can be extended to humanoid hopping robot as follows. Hopping robot can be considered as a redundant manipulator with a load held at the end-effector (Kurazume and Hasegawa, 2006). Figure 2 shows the hopping robot and inertia matching ellipsoid (IME).

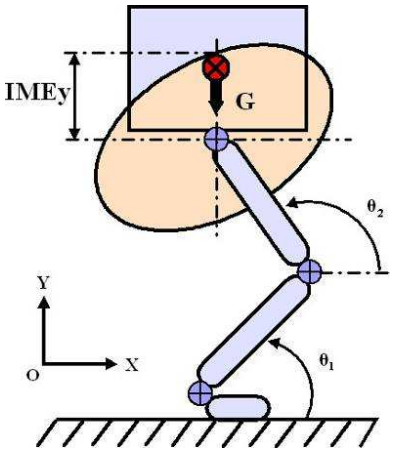


**Figure 2. Hopping robot model and inertia matching ellipsoid.**

The motion and force equation analyzing to the load held at the end-effector can be written as

$$\mathbf{F}_e = m_l\left(\ddot{\mathbf{R}}_E + \mathbf{g}\right) \tag{1}$$

where $\mathbf{R}_E$ is the position vector of the end-effector, $m_l$ is the mass inertia of load, $\mathbf{g}=(0,-g)^T$ is the gravity vector. The end-effector posture of manipulator $\mathbf{R}_E$ is related to the shape of the robot $\boldsymbol{\theta}$ as follows:

$$\begin{cases}\mathbf{R}_E=[\mathbf{X}_E \quad \mathbf{Y}_E]^{\mathrm{T}}=\mathbf{E}_E(\boldsymbol{\theta})\\ \dot{\mathbf{R}}_E=\mathbf{J}(\boldsymbol{\theta})\dot{\boldsymbol{\theta}}\\ \ddot{\mathbf{R}}_E=\mathbf{J}(\boldsymbol{\theta})\ddot{\boldsymbol{\theta}}+\dot{\mathbf{J}}(\boldsymbol{\theta})\dot{\boldsymbol{\theta}}\end{cases} \tag{2}$$

where $\mathbf{J}(\boldsymbol{\theta})$ is Jacobian matrix.

Hopping performance is affected by any motion control and hopping posture. Hopping posture affects not only the attitude during flight phase, but the angular momentum with respect to COG. Dynamics model can be derived by some methods, such as Newton-Euler equations, Lagrange equations, Gauss and Kane methods. In this paper, the dynamics model is established by applying Lagrange equations. When an external moment/force is applied to the hopping robot, dynamics equation during stance phase can be written as

$$\mathbf{D}_s(\boldsymbol{\theta})\ddot{\mathbf{q}}+\mathbf{H}_s\left(\boldsymbol{\theta},\dot{\boldsymbol{\theta}}\right)\dot{\mathbf{q}}+\mathbf{G}_s(\boldsymbol{\theta})+\mathbf{J}(\boldsymbol{\theta})^{\mathrm{T}}\mathbf{F}_e=\mathbf{B}_s\boldsymbol{\Gamma}_s \tag{3}$$

where, $\mathbf{D}_s(\boldsymbol{\theta})$ is an inertia matrix, which is symmetric and positive define. $\mathbf{H}_s\left(\boldsymbol{\theta},\dot{\boldsymbol{\theta}}\right)$ is a centrifugal matrix which contains the centrifugal acceleration and Coriolis terms. $\mathbf{G}_s(\boldsymbol{\theta})$ is a gravitational vector, $\mathbf{B}_s$ is a matrix $\begin{bmatrix}-1 & 1 & 0\\ 0 & -1 & 1\\ 0 & 0 & -1\end{bmatrix}$, and $\boldsymbol{\Gamma}_s$ is external torque vector $\begin{bmatrix}\tau_F^f & \tau_K^f & \tau_H^f\end{bmatrix}^T$.

Substituting Eqs. (1) and (2) into (3), the torque matrix can be obtained by

$$\begin{aligned}\boldsymbol{\Gamma}_s &= \mathbf{B}_s^{\dagger}\left[\mathbf{D}_s(\boldsymbol{\theta})\mathbf{J}(\boldsymbol{\theta})^{\dagger}\left(\mathbf{F}_e-m_l\mathbf{g}-m_l\dot{\mathbf{J}}(\boldsymbol{\theta})\dot{\mathbf{q}}\right)/m_l+\mathbf{H}_s\left(\boldsymbol{\theta},\dot{\boldsymbol{\theta}}\right)\dot{\mathbf{q}}+\mathbf{G}_s(\boldsymbol{\theta})+\mathbf{J}(\boldsymbol{\theta})^{\mathrm{T}}\mathbf{F}_e\right]\\ &= \mathbf{Q}(\boldsymbol{\theta})\left(\mathbf{F}_e-\mathbf{F}_{bias}\right)\end{aligned} \tag{4}$$

Where

$$\begin{cases}\mathbf{Q}(\boldsymbol{\theta})=\mathbf{B}_s^{\dagger}\left[\mathbf{J}(\boldsymbol{\theta})^T+\mathbf{D}_s(\boldsymbol{\theta})\mathbf{J}(\boldsymbol{\theta})^{\dagger}/m_l\right]\\ \mathbf{F}_{bias}=\mathbf{W}\left(\mathbf{J}(\boldsymbol{\theta})^T+\mathbf{D}_s(\boldsymbol{\theta})\mathbf{J}(\boldsymbol{\theta})^{\dagger}/m_l\right)^{\dagger}\times\\ \qquad\left[\mathbf{D}_s(\boldsymbol{\theta})\mathbf{J}(\boldsymbol{\theta})^{\dagger}\left(\mathbf{g}+\dot{\mathbf{J}}(\boldsymbol{\theta})\dot{\mathbf{q}}\right)-\mathbf{H}_s\left(\boldsymbol{\theta},\dot{\boldsymbol{\theta}}\right)\dot{\mathbf{q}}-\mathbf{G}_s(\boldsymbol{\theta})\right]\end{cases} \tag{5}$$

Here, $\mathbf{F}_{bias}$ is a bias force matrix of angular velocity and acceleration. $\mathbf{F}_e-\mathbf{F}_{bias}$ is inertia matching for hopping robot. $\mathbf{J}(\boldsymbol{\theta})^{\dagger}$ is a pseudoinverse of the Jacobian matrix $\mathbf{J}(\boldsymbol{\theta})$. When the Jacobian matrix is a regular matrix, then $\mathbf{J}(\boldsymbol{\theta})^{\dagger}=\mathbf{J}(\boldsymbol{\theta})^{-1}$. In the case that Jacobian matrix is a rectangular matrix, then $\mathbf{J}(\boldsymbol{\theta})^{\dagger}=\mathbf{W}^{-1}\mathbf{J}(\boldsymbol{\theta})^T\left(\mathbf{J}(\boldsymbol{\theta})\mathbf{W}^{-1}\mathbf{J}(\boldsymbol{\theta})^T\right)^{-1}$, where $\mathbf{W}$ is a weight matrix. The coefficient matrix $\mathbf{Q}(\boldsymbol{\theta})$ indicates the moment or force transmission efficiency between the torque produced at the actuators and the force or moment applied to the load by the end-effector.

Based on the theory of singular value decomposition (SVD), $\mathbf{Q}(\boldsymbol{\theta})$ can be given by

$$\mathbf{Q}(\boldsymbol{\theta})=\mathbf{U}\boldsymbol{\Sigma}\mathbf{V}^T \tag{6}$$

where $\mathbf{U}\in\mathbf{R}^{m\times n}$ and $\mathbf{V}\in\mathbf{R}^{n\times n}$ are orthogonal matrices, $\boldsymbol{\Sigma}=diag(\sigma_1,\sigma_2,\cdots,\sigma_m)\in\mathbf{R}^{m\times n}$, and $\sigma_i$ is a nonnegative singular value.

The manipulability measure $\omega$ of inertia matching $\mathbf{F}_e - \mathbf{F}_{bias}$ can be expressed as the product of $\sigma_i$ :

$$\omega = \sigma_1 \cdot \sigma_1 \cdots \sigma_m \tag{7}$$

The principal axes are the product between the row vector $(u_1,\cdots,u_m)$ of $\mathbf{U}$ and the singular value vector $(\sigma_1,\cdots,\sigma_m)$ . And moreover, the singular value vector $(\sigma_1,\cdots,\sigma_m)$ shows the motion capability of the corresponding principal axis. The manipulability measure of inertia matching synthetically evaluates the isotropic flexibility of robot, and it measures the manipulability of manipulator as a whole.

Hopping motion includes various hopping forms, such as vertical hopping and long hopping. In order to achieve hopping task (jump over an obstacle), directional manipulability measure of inertia matching is proposed.

Assuming the moment and force vector applied to the center of load at end-effector is given by

$$\mathbf{F}_e - \mathbf{F}_{bias} = A_{IM}\mathbf{P} \tag{8}$$

where $A_{IM}$ is the scalar quantity form of inertia matching $\mathbf{F}_e - \mathbf{F}_{bias}$ , $\mathbf{P}$ is the direction of the force in load at end-effector in Cartesian frame, and $\mathbf{P} = (\cos\beta_1, \cos\beta_2, \cdots, \cos\beta_n)^T \in \mathbf{R}^{n\times 1}$ , $\beta_i$ is the angle between inertia matching and the positive horizontal axis.

Substituting Eqs. (8) into (4), the following equation can be obtained

$$\mathbf{\Gamma}_s = A_{IM}\mathbf{Q}(\boldsymbol{\theta})\mathbf{P} \tag{9}$$

Generally, the torque limits at each actuator in hopping robot are assumed to be symmetrical and constrained, viz $-\tau_{i\max} \le \tau_i \le \tau_{i\max}$ . The normalized joint torque $\tilde{\mathbf{\Gamma}}$ can be obtained using a conversion matrix $\mathbf{L} = diag(\tau_{1\max},\cdots,\tau_{n\max})$ as

$$\tilde{\mathbf{\Gamma}} = \mathbf{L}^{-1}\mathbf{\Gamma} \tag{10}$$

Therefore, when a normalized torque with magnitude of 1 is produced, the inertia matching ellipsoid can be obtained as

$$A_{IM}^2 \mathbf{P}^T \mathbf{Q}^T(\boldsymbol{\theta})\mathbf{L}^{-2}\mathbf{Q}(\boldsymbol{\theta})\mathbf{P} \le 1 \tag{11}$$

The directional manipulability of inertia matching can be given by

$$DM_{IM} = A_{IM}^2 \le \left[\mathbf{P}^T \mathbf{Q}^T(\boldsymbol{\theta})\mathbf{L}^{-2}\mathbf{Q}(\boldsymbol{\theta})\mathbf{P}\right]^{-1} \tag{12}$$

The directional manipulability measure of inertia matching $DM_{IM}$ reflects the manipulability in specified direction of robot.

Analyzed the hopping robot as a whole, hopping height is determined by take-off velocity, and the COG trajectory after take-off is a parabola. During take-off motion, the angle between $\overline{\mathbf{FG}}$ and horizontal axis is defined as jumping angle $\theta_{jump}$ , and it can be regarded as a process from the initial posture $\theta_{jump\_i} = f_{jump}(\theta_1^{td},\theta_2^{td},\theta_3^{td})$ to the ultimate posture $\theta_{jump\_u} = f_{jump}(\theta_1^{to},\theta_2^{to},\theta_3^{to})$ through the harmonious movement of joints. Moreover, there is only one constraint function which including three variable parameters. So there is a redundant parameter $\theta_3$ . In this paper, the upper body posture $\theta_3$ is constrained to fluctuate around $\pi/2$ . The jumping angle is determined by hopping task. For example, long jumping has a jumping angle which can decide the long distance. Jumping over an obstacle, the jumping angle should satisfy a certain function.

The manipulability measure of inertia matching is a function of posture $\boldsymbol{\theta}$ , and it reflects the moment/force transmission efficiency between the torque produced at the actuators and the force or moment applied to the load by the end-effector. The take-off posture is a main factor which affects hopping performance. When the force transmission efficiency of interior joints is maximal, the time integral of ground reaction force will reach the maximization, so the hopping height is maximal. Applied the inertia matching and directional manipulability, the posture optimization of hopping motion can be denoted by

$$\begin{aligned} &\max \quad \left[\mathbf{P}^T \mathbf{Q}^T(\boldsymbol{\theta})\mathbf{L}^{-2}\mathbf{Q}(\boldsymbol{\theta})\mathbf{P}\right]^{-1} \\ &\text{s. t} \quad \theta_{jump} = f_{jump}(\theta_1,\theta_2,\theta_3) \end{aligned} \tag{13}$$

where, constraint function $f_{jump}(\theta_1,\theta_2,\theta_3)$ is determined by an obstacle, and in order to avoid redundancy, the take-off posture of upper body is constrained to fluctuate around $\pi/2$ .

## Trajectory Planning for Jumping over Obstacles

The take-off postures, viz $\theta_1^{to}$ , $\theta_2^{to}$ and $\theta_3^{to}$ , is established by the optimization results with inertia matching and directional manipulability. The touch-down postures, viz $\theta_1^{td}$ , $\theta_2^{td}$ and $\theta_3^{td}$ , are given by desired parameters. The trajectory planning satisfies dynamics constraints and boundary conditions. The motion of body is established by internal motion dynamics and steady-state consecutive hopping motion principle

Based on the kinematics of the robot, the relationship between the COG position and the foot F position can be expressed as

$$\begin{bmatrix}\mathbf{R}_G\\ \dot{\mathbf{R}}_G\\ \ddot{\mathbf{R}}_G\end{bmatrix} - \begin{bmatrix}\mathbf{R}_F\\ \dot{\mathbf{R}}_F\\ \ddot{\mathbf{R}}_F\end{bmatrix} = \begin{bmatrix}\mathbf{E}_G(\boldsymbol{\theta})\\ \mathbf{J}\dot{\boldsymbol{\theta}}\\ \mathbf{J}\dot{\boldsymbol{\theta}} + \mathbf{J}\ddot{\boldsymbol{\theta}}\end{bmatrix} \tag{14}$$

where $\mathbf{R}_G = [\mathbf{X}_G, \mathbf{Y}_G]^T$ , $\mathbf{R}_F = [\mathbf{X}_F, \mathbf{Y}_F]^T$ .

The parameters of obstacles are described by height $H_o$ and length $L_o$ . In order to lift foot over the obstacle, jumping height can be evaluated as follows:

$$\begin{cases} H_{jump} = \mathbf{E}_H(H_o,\boldsymbol{\theta}) \\ L_{jump} = X_F^{td} - X_F^{to} = \mathbf{E}_L(H_o,L_o,\boldsymbol{\theta}) \end{cases} \tag{15}$$

Suppose that at take-off the foot does not slip. The velocity of the foot **F** at touch-down is given by input parameter $k_i$ , it reflects the amount of kinetic energy loss during impact. If trajectory is a soft landing, $k_i$ is zero. The acceleration of the foot at touch-down has an influence on the amplitude of the ground reaction force immediately after impact. The velocity and acceleration of the foot at touch-down will be defined here proportional to the velocity of the COG. So yields

$$\begin{cases} \dot{X}_F^{to} = 0 & \dot{X}_F^{td} = k_1\dot{X}_G^{td} \\ \dot{Y}_F^{to} = 0 & \dot{Y}_F^{td} = k_2\dot{Y}_G^{td} \\ \ddot{X}_F^{to} = 0 & \ddot{X}_F^{td} = k_3\ddot{X}_G^{td} \\ \ddot{Y}_F^{to} = 0 & \ddot{Y}_F^{td} = k_4\ddot{Y}_G^{td} \end{cases} \tag{16}$$

During the ballistic flight phase the COG tracks a parabolic trajectory. The flight time can be expressed as following by the initial conditions

$$\begin{cases} T^{fl} = \mathbf{E}_{T-H}\left(H_{jump}, \mathbf{R}_G^{tj}\right) \\ \dot{Y}_G^{to} = \mathbf{E}_{Y-H}\left(H_{jump}\right) \\ \dot{\mathbf{R}}_G^{td} = \mathbf{E}_{R-HL}\left(L_{jump}, H_{jump}, \mathbf{R}_G^{tj}, \boldsymbol{\theta}^{tj}\right) \end{cases}, (tj = to, td) \tag{17}$$

The angular momentum with respect to COG can be calculated with the following general formula:

$$\mu_G^f = \sum_{i=1}^{3}\left(\overline{GG_i} \times m_i \overline{GG_i}' + I_i\dot{\theta}_i\right) = \sum_{i=1}^{3} f_{\mu i}(\theta_i)\dot{\theta}_i \tag{18}$$

When the angular momentum is denoted by absolute angle $\boldsymbol{\theta}$, $f_{\mu i}(\theta_i)$ is a function of parameters $\theta_1$, $\theta_2$ and $\theta_3$. Defined two relative angles $q_1 = \theta_2 - \theta_1$ and $q_2 = \theta_3 - \theta_2$. The vector $\mathbf{q}$ is the relative angle $(q_1, q_2, q_3)^T$. The angular momentum with respect to COG can be expressed as

$$\mu_G^f = \sum_{i=1}^{3} f_{\mu i}(\mathbf{q})\dot{q}_i \tag{19}$$

where $f_{\mu i}(\mathbf{q})$ is a function of parameters only $q_1$ and $q_2$.

During the flight phase, the leg will swing forward in order to position the foot on a chosen foothold. Because of the angular momentum constraint the body will rotate too. At touch-down the body will have orientation $\theta_3^{td}$ and an angular velocity $\dot{\theta}_3^{td}$. The take-off conditions will have to be chosen in such a way that the orientation and velocity of the body at touch-down equalize these desired values. Given a value $\dot{\theta}_3^{td,0}$ at random, and based on COG parabolic trajectory during flight phase, velocity and acceleration can be written as

$$\begin{bmatrix} \dot{\mathbf{q}}^{tj} \\ \ddot{\mathbf{q}}^{tj} \end{bmatrix} = \mathbf{E}_{q-q}(\mathbf{q})\begin{bmatrix} \mathbf{q}^{tj} \\ \dot{\mathbf{q}}^{tj} \end{bmatrix} + \mathbf{E}_{q-R}(\mathbf{q})\begin{bmatrix} \mathbf{R}_G^{tj} \\ \dot{\mathbf{R}}_G^{tj} \end{bmatrix}, (tj = to, td) \tag{20}$$

Since now boundary conditions at take-off as well as at touch-down are known for both the angles $q_i\,(i = 1,2)$ and their first and second derivatives. Normally, a 5th order polynomial tracking function can be established for $q_i$ under their position, velocity, and acceleration constraints of both initial point and ultimate point. It is the traditional point-to-point motion planning.

$$\tilde{q}_i^f = \sum_{j=0}^{5} a_i t^j \ , \ (i = 1,2) \tag{21}$$

There is a problem: since the operational time is determined by initial and ultimate conditions such as flight, the polynomial is sensitive to the initial point or ultimate constraint conditions by using a 5th order polynomial to track trajectory. If one condition changes among the six constraint conditions, the trajectory would change very large. Moreover, the trajectory would not satisfy the angular work space. Figure 3 shows the trajectory which is planned by using a 5th order polynomial after changed initial condition have exceeded maximum work space $\pi/2$.

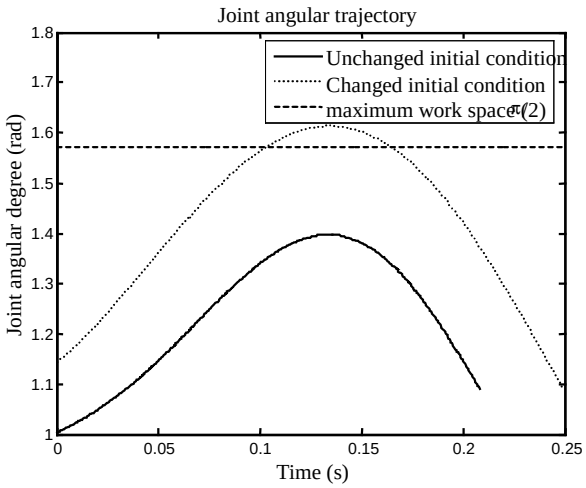


**Figure 3. Trajectory using a 5th order polynomial under before-change initial condition and after-change initial condition.**

Aimed at this problem, and in order to enhance the trajectory generation efficiency and improve the trajectory robustness to constraint conditions, a 6th polynomial is proposed to track trajectory

$$\tilde{q}_i^f = \sum_{j=0}^{6} a_i t^j \ , \ (i = 1,2) \tag{22}$$

The highest power coefficient $a_6$ is obtained by joint motion constraints, the other power coefficients are determined by the initial and ultimate constraint conditions. The trajectory can be ensured to satisfy the joint workspace through the optimization of the 6th power coefficient because the highest power polynomial coefficient is most sensitive and influencing to the shape of a polynomial. If the highest power coefficient is ascertained, the trajectory polynomial will have a little influence with the change of the other lower power coefficients. Thus, this polynomial has a good robustness for the constraint conditions. Figure 4 shows the trajectory which is planned by using a 6th order polynomial after changed initial condition is also under maximum work space $\pi/2$.

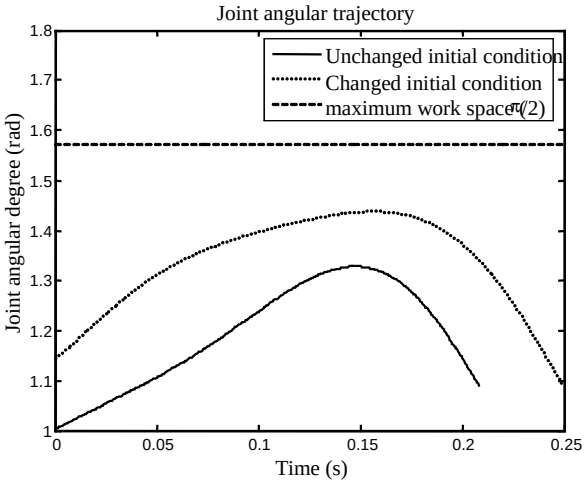


**Figure 4. Trajectory using a 6th order polynomial under before-change initial condition and after-change initial condition.**

After obtaining the trajectory $\tilde{q}_1^f$ and $\tilde{q}_2^f$, the posture of upper body can be obtained based on angular momentum theory

$$\begin{cases} \dot{\theta}_3 = \left[\mu_G^f - f_{\mu 1}(\mathbf{q})\dot{q}_1 - f_{\mu 2}(\mathbf{q})\dot{q}_2\right] / f_{\mu 3}(\mathbf{q}) \\ \theta_{3,real} = \theta_3^{to} + \int_{t_{to}}^{t} \dot{\theta}_3 dt \\ \theta_{3,real}^{td} = \theta_3^{to} + \int_{t_{to}}^{td} \dot{\theta}_3 dt \end{cases} \tag{23}$$

The angle $\theta_{3,real}^{td}$ differs from the desired value $\theta_3^{td}$ because of the initial value $\dot{\theta}_3^{td,0}$. In order to control the upper body posture to the desired value, $\dot{\theta}_3^{td}$ can be adjusted by an iterative method

$$\dot{\theta}_3^{td,n+1} = \dot{\theta}_3^{td,n} + \left(\theta_3^{td} - \theta_{3,real}^{td}\right) / T^{fl} \tag{24}$$

The polynomial function $\theta$ is completely determined by the boundary points only. In order to lift foot over the obstacle, a correction on the polynomial function is introduced. An intermediate point is added to the polynomial function to make sure that the foot reaches the height of obstacle at $t = t^*$, where $t^*$ is the time step where G and foot reach their maximum height at the same time.

$$\begin{cases} \dot{Y}_G(t^*) = 0 \\ \dot{Y}_F(t^*) = 0 \end{cases} \tag{25}$$

This strategy is chosen here, since it results in an analytical solution for the correction functions. A correction function $b_i(t)(i = 1,2)$ will be added, which does not change the boundary conditions of the polynomial functions $\tilde{q}_i^f$.

$$\begin{cases} b_i(t) = K_i f_{co}(t) \\ f_{co}(t) = \dfrac{t^3\left(T^{fl} - t\right)^3}{\left(t^*\right)^3\left(T^{fl} - t^*\right)^3} \end{cases} \tag{26}$$

Based on parabolic motion of COG of the robot, $K_i$ can be solved as the following set:

$$\begin{cases} Y_G(t^*) = Y_G^{to} + \dot{Y}_G^{to}\left(t^* - t_{to}\right) - \dfrac{g\left(t^* - t_{to}\right)^2}{2} \\ \dot{Y}_G(t^*) = 0 \end{cases} \tag{27}$$

Thus, the angular value $q_i^f$ can be devoted by the polynomial function $\tilde{q}_i^f$ and correction function $b_i(t)$ as follows:

$$q_i^f = \tilde{q}_i^f + b_i(t), \ (i = 1,2) \tag{28}$$

Using Eq. (23), the upper body trajectory after considering correction functions can be obtained. The absolute angle trajectory $\boldsymbol{\theta}$ can be found through the relation between absolute angles and relative angles.

Because of the constraints on the leg during stance demanding that the foot should stay at a fixed position, the polynomial functions during stance phase can be constructed by using the results of impact phase and take-off posture. As a steady-state consecutive hopping, the final conditions during stance phase are equal to the initial conditions at take-off during flight phase. The initial conditions during stance phase are equal to the conditions after impact, and the conditions before impact are equal to the final conditions during flight phase respectively.

$$\begin{cases} \boldsymbol{\theta}^{so} = \boldsymbol{\theta}^{+} & \boldsymbol{\theta}^{sd} = \boldsymbol{\theta}^{to} & \boldsymbol{\theta}^{-} = \boldsymbol{\theta}^{td} \\ \dot{\boldsymbol{\theta}}^{so} = \dot{\boldsymbol{\theta}}^{+} & \dot{\boldsymbol{\theta}}^{sd} = \dot{\boldsymbol{\theta}}^{to} & \dot{\boldsymbol{\theta}}^{-} = \dot{\boldsymbol{\theta}}^{td} \\ \ddot{\boldsymbol{\theta}}^{so} = \ddot{\boldsymbol{\theta}}^{+} & \ddot{\boldsymbol{\theta}}^{sd} = \ddot{\boldsymbol{\theta}}^{to} & \ddot{\boldsymbol{\theta}}^{-} = \ddot{\boldsymbol{\theta}}^{td} \end{cases} \tag{29}$$

where the superscript $^{sd}$ denotes ultimate state configuration during stance phase, the superscript $^{+}$ denotes the state configuration after impact, and the superscript $^{-}$ denotes the state configuration before impact.

At the landing, the foot of the hopper hits the ground. Let's assume the foot doesn't bounce back and doesn't slip, which means that it stays in contact with the ground. These are the assumptions corresponding to an inelastic impulsive impact. During this impact phase, although discontinuities in the velocity and acceleration state variables will occur, the configuration of the robot is assumed to stay unchanged,

$$\boldsymbol{\theta}^{+} = \boldsymbol{\theta}^{-} \tag{30}$$

According to Zheng and Hemami (1985) the discrete variation of the generalized velocities due to the inelastic impulsive impact with the ground can be calculated as follows:

$$\Delta\dot{\mathbf{q}} = \mathbf{D}_f^{-1}(\boldsymbol{\theta})\mathbf{J}^T\left(\mathbf{J}\mathbf{D}_f^{-1}(\boldsymbol{\theta})\mathbf{J}^T\right)^{-1}\Delta\overrightarrow{\mathbf{OF}} \tag{31}$$

with $\Delta\dot{\mathbf{q}} = \left(\Delta\dot{\boldsymbol{\theta}}, \Delta\dot{\theta}_3, \Delta\dot{X}_F, \Delta\dot{Y}_F\right)^T$ and $\Delta\overrightarrow{\mathbf{OF}} = \left(\Delta\dot{X}_F, \Delta\dot{Y}_F\right)^T$.

From the Eq. (31), the velocity after impact can be expressed as

$$\begin{bmatrix} \dot{\theta}_1^{+} \\ \dot{\theta}_2^{+} \\ \dot{\theta}_3^{+} \end{bmatrix} = \begin{bmatrix} \dot{\theta}_1^{td} \\ \dot{\theta}_2^{td} \\ \dot{\theta}_3^{td} \end{bmatrix} - \mathbf{D}_f^{-1}(\boldsymbol{\theta})\mathbf{J}^T\left(\mathbf{J}\mathbf{D}_f^{-1}(\boldsymbol{\theta})\mathbf{J}^T\right)^{-1}\begin{bmatrix} \dot{X}_F^{td} \\ \dot{Y}_F^{td} \end{bmatrix} \tag{32}$$

To calculate the angular accelerations $\ddot{\boldsymbol{\theta}}^{+}$ after impact, the equation of motion for the stance phase can be used. The joint torques is considered to remain unchanged during the infinitesimal short time interval of the impact. Their values are those measured at the instance of landing impact

$$\begin{cases} \tau_F^{so} = \tau_F^{td} \\ \tau_K^{so} = \tau_K^{td} \\ \tau_H^{so} = \tau_H^{td} \end{cases} \tag{33}$$

From the Eq. (33), the angular accelerations after impact can be expressed as

$$\ddot{\boldsymbol{\theta}}_s^{+} = \left(\mathbf{D}_s^{so}\right)^{-1}\left(\mathbf{D}_f^{td}\ddot{\mathbf{q}}^{td} + \mathbf{H}_f^{td}\dot{\mathbf{q}}^{td} + \mathbf{G}_f^{td} - \mathbf{H}_s^{so}\dot{\mathbf{q}}^{so} - \mathbf{G}_s^{so}\right) \tag{34}$$

During flight phase, the angular momentum with respect to COG $\mu_G^f$ is conserved without external forces acting on the robot, and the angular momentum with respect to foot $\mu_F^f$ can be obtained by $\mu_G^f$. During stance phase, there are the external ground reaction forces on the foot, and the angular momentum with respect to foot $\mu_F^s$ can be obtained by integration over the stance time

$$\begin{cases} \mu_F^f = \mu_G^f + \overline{\mathbf{FG}}^f \times M\overline{\mathbf{FG}}'^f \\ \mu_F^s = \mu_F^{td} + Mg\int_{t_{to}}^{t}(X_G - X_F)dt \end{cases} \tag{35}$$

The stance time $T^{st}$ can be calculated by Eq. (35) as follows:

$$Mg\int_{t_{to}}^{t_{td}} X_G dt = \overline{\mathbf{FG}}^{to} \times M\overline{\mathbf{FG}}'^{to} - \overline{\mathbf{FG}}^{td} \times M\overline{\mathbf{FG}}'^{td} \tag{36}$$

After obtained six boundary conditions and stance time, in an analogue way as during flight, 6th order polynomials can be calculated, which are the reference trajectories $\theta_i^{st}$ for lower leg, upper leg and upper body respectively during stance phase.

## Simulations and Experiments

A hopping robot which has 3-DOF rotary joints and four rigid bodies (foot, lower leg, upper leg, upper body) is designed. Figure 5 shows the one-legged model, and its inertia parameters are given in Table 1. The ankle, knee and hip joints are independently driven by servo motors. The type of servo motors is GWS S777, which is made in Taiwan, China. Its rated velocity is 0.12 *s*/60° (6.0*V*), viz 8.72 *rad/s*, and its rated torque is 42 *kgcm*. In this robot model, there are not any assistant elastic components, such as spring, damp, hydraulic or pneumatic actuators. The controller is an AVR system, and main control chip is Atmega128 from ATMEL company. The ATmega128 is a low-power CMOS 8-bit microcontroller based on the AVR enhanced RISC architecture. It provides four flexible Timer/Counters with compare modes and PWM, and PWM can directly drive servo motor.

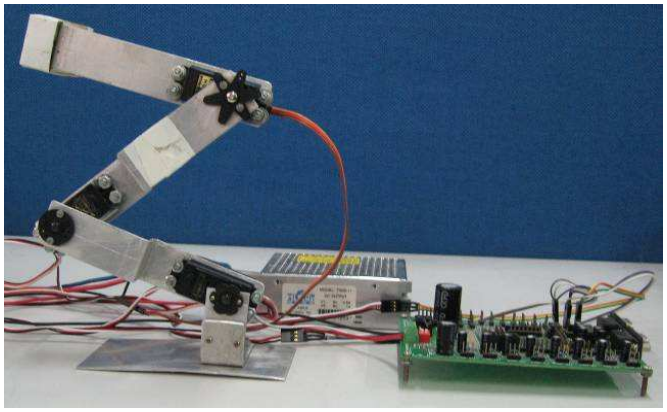

**Figure 5. One-legged hopping robot prototype.**

**Table1. Inertial parameters of the hopping robot.**

| $i$ | $L_i(m)$ | $\alpha_i$ | $m_i(kg)$ | $I_i(kg\cdot m^2)$ | $\tau_i(kg\cdot cm)$ |
|---|---|---|---|---|---|
| 1 | 0.34 | 0.85 | 0.178 | $1.38\times10^{-3}$ | 42 |
| 2 | 0.31 | 0.55 | 0.137 | $2.18\times10^{-3}$ | 42 |
| 3 | 0.37 | 0.15 | 0.851 | $7.98\times10^{-3}$ | 42 |

The parameters of obstacle and postures at touch-down are the following:

$$H_o = 0.01m,\ L_o = 0.01m,\ \theta_1^{td} = 1.35rad,\ \theta_2^{td} = 2.15rad,\ \theta_3^{td} = 1.40rad$$

Figure 6 shows a stick diagram for steady-state consecutive hopping motion. The solid line denotes a sequence of hopping movement including flight phase and stance phase. The dashed line is a steady-state consecutive hopping performance.

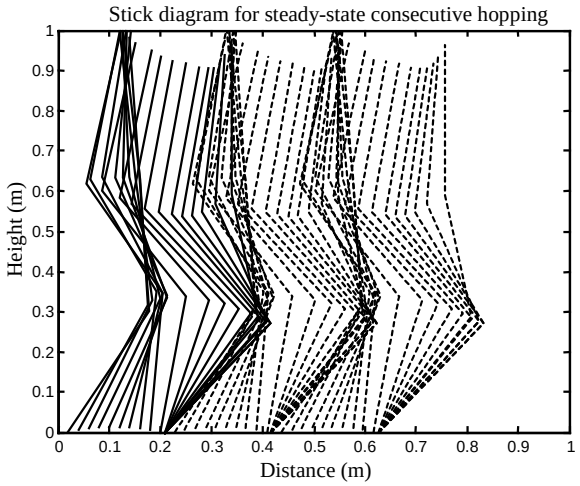


**Figure 6. Stick diagram for steady-state consecutive hopping.**

Figure 7 shows inertia matching under different take-off postures by simulation, and Figure 8 is hopping height under different take-off postures by experiments. Inertia matching and hopping height both reach a maximization when $\theta_1$ is equal to 1.01*rad*. Here, $\theta_2$ which can be obtained with jumping angle is 1.74*rad* based on the size of the obstacle.

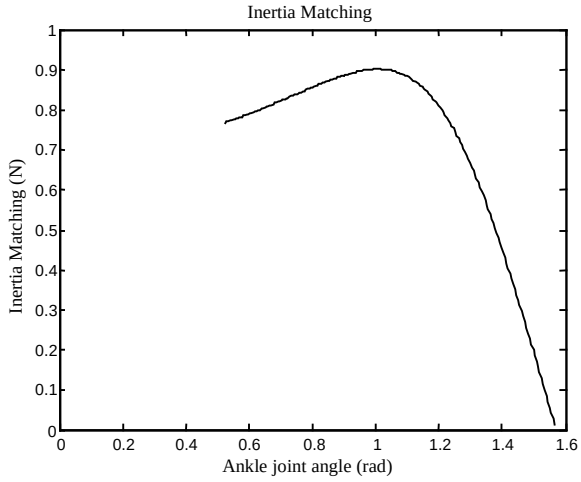


**Figure 7. Inertia matching under different take-off postures by simulation.**

In view of force transmission efficiency and the time integral of ground reaction force, hopping height is in direct proportion to the time integral of ground reaction force. Figure 9 shows ground reaction force under different postures by simulation. When take-off posture is in the optimization, the time integral of ground reaction force and hopping height are maximal. When the angular angle of ankle increases from 0.52*rad* to 1.01*rad*, inertia matching gradually increases to the maximal 0.9N, the hopping height gradually increases to the maximal 0.014m, and the ground reaction force also gradually increases to the maximum 17.8N. When the angular angle of ankle is on the increase, inertia matching rapidly reduces to zero, the hopping height rapidly reduces to zero, and the ground reaction force also rapidly reduces. Thus inertia matching is in direct proportion to hopping height/hopping performance, and it can be applied to analyze the hopping motion.

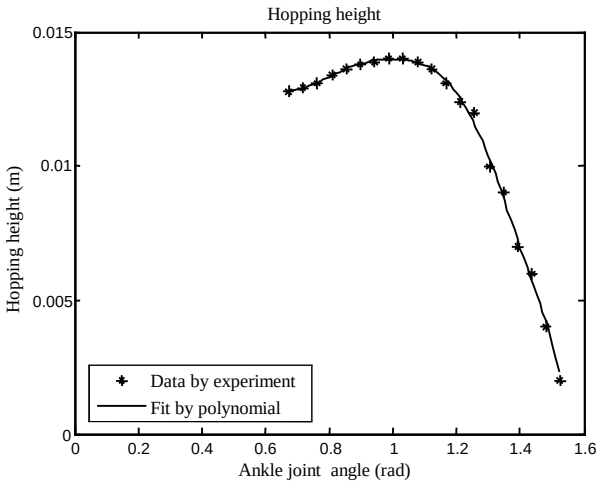


**Figure 8. Hopping height under different take-off postures by experiments.**

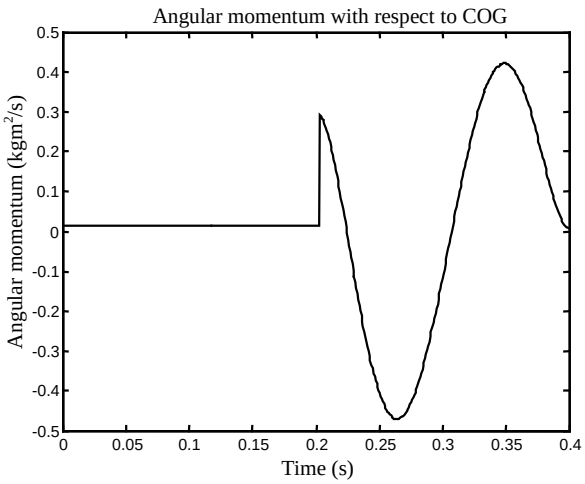


**Figure 10. Angular momentum trajectory with respect to COG.**

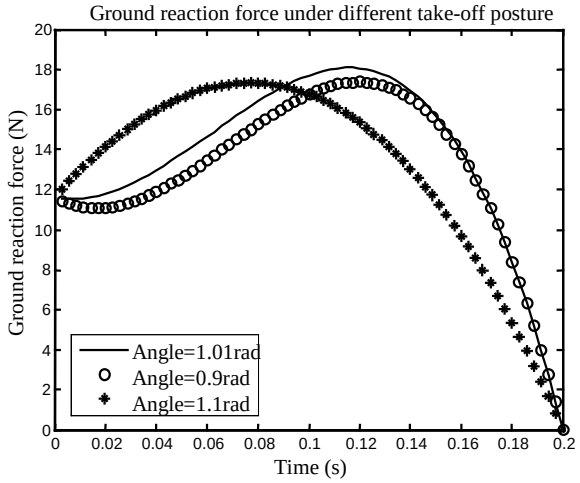


**Figure 9. Distributing of ground reaction force under different postures by simulation.**

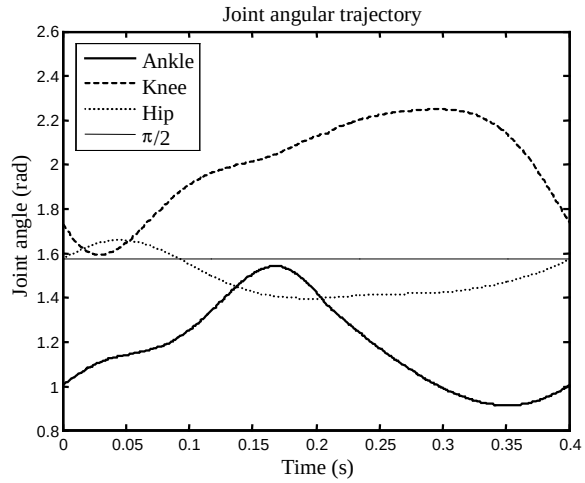


**Figure 11. Joint angle trajectory of lower leg, upper leg and body.**

The trajectories tracked by the actuators of the leg during the stance phase, which guarantee that the desired values for jumping over the obstacle are attained, cause a clockwise natural rotation of upper body. Therefore a counterclockwise rotation of upper body during the fight phase is suitable, since these both rotations can compensate each other. Figure 10 shows the angular momentum with respect to COG is 0.012 $kgm^2/s$ during the flight phase.

Figure 11 shows that using proposed 6th polynomial functions, the joint angle trajectory is all under the joint workspace. From Figure 12, the peak values among those three angular torques are smaller than the rate torque value 4.1*Nm* of servomotor. The peak value of the knee torque is significantly higher than others, being approximately 4*Nm* during the stance phase. The torque at ankle is very small, it indicates the dynamic stability under planning trajectories is satisfactory to actual motor performance.

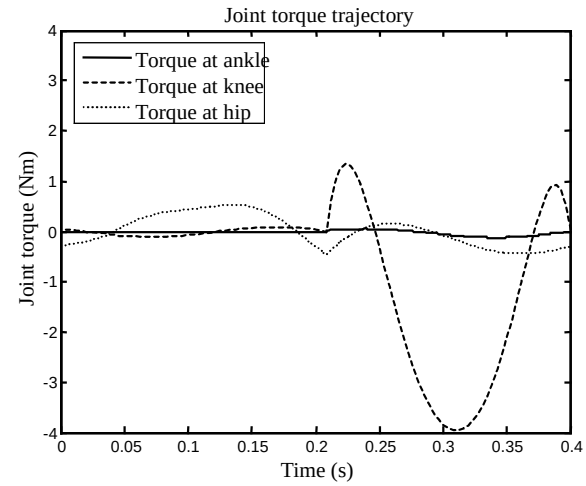


**Figure 12. Torque trajectory at knee and hip.**

Figure 13 shows the vertical position of the foot using with/without correction function. It shows that the foot can over the designed obstacle after using correction function.

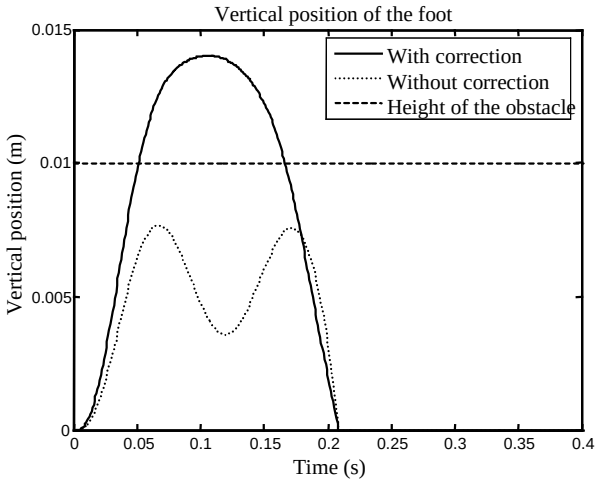


**Figure 13. Vertical position of foot.**

## Conclusions

Trajectory planning strategy for a one-legged multi-jointed hopping robot is developed. The take-off postures which are optimized by inertia matching and directional manipulability are used to plan hopping trajectory. Moreover, aimed at point-to-point motion, 6th order polynomials are proposed to track the joint trajectory. They have a better robustness to the changed constraint conditions than traditional 5th polynomial. This method improves the efficiency of trajectory generation. Furthermore, the angular momentum is decoupled using relative joints, and the upper body trajectory is solved with angular momentum theory and iterative method during flight phase. In order to lift the foot to jump over the designed obstacles, a correction function is constructed under unchanged boundary constraint conditions. Finally, the robot postures are planned with internal motion dynamics and steady-state consecutive hopping motion.

Hopping robot is a hybrid system including holonomic and non-holonomic constraints, the contents of dynamics and control are very wide. In this paper, trajectory planning control is only in view of boundary constraint conditions and internal motion dynamics. In the future, postural stability, softy landing and natural passive dynamics will be focused.

## Acknowledgments

The authors gratefully acknowledge the support of this research by China Scholarship Council (CCS). The authors would like to thank facilities of Engineering Training Center and Mechanical department in Shanghai Jiao Tong University (SJTU). The authors also thank the anonymous reviews for improving the quality of the paper.

## References

Babic, J. and Omrcen, D., 2006, "Stability control of human inspired jumping robot", Proc. of 15th International Workshop on Robotics in Alpe-Adria-Danube Region, pp. 206-211.

Bowling, A. and Khatib, O., 2005, "The dynamic capability equations: a new tool for analyzing robotic manipulator performance", *IEEE Transactions on Robotics*, 21(1), pp. 115-123.

Chen, D.Z. and Tsai, L.W., 1991, "The generalized principle of inertia match for geared robotic mechanisms", Proc. of the IEEE International Conference on Robotics and Automation, Sacramento, CA, pp. 1282-1287.

De Man, H., Lefeber, D. and Vermeulen, J., 1998, "Design and Control of a Robot with One Articulated Leg for Locomotion on Irregular Terrain", Proc. of 12th Symposium on Theory and Practice of Robots and Manipulators, New York, pp. 417-424.

Kurazume, R. and Hasegawa, T., 2006, "A New Index of Serial-Link Manipulator Performance Combining Dynamic Manipulability and Manipulating Force Ellisoids", *IEEE Transactions on Robotics*, 22(5), pp. 1022-1028.

Li, Z. and Montgomery, R., 1990, "Dynamics and Optimal Control of a Legged Robot in Flight Phase", Proc. of IEEE International Conference on Robotics and Automation, Cincinnati, USA, pp. 1816-1821.

Ohashi, E. and Ohnishi, K., 2006, "Hopping height control for hopping robots", Electrical Engineering in Japan, Vol. 155(1), pp. 64-71.

Vermeulen, J., Lefeber, D. and Verrelst B., 2003, "Control of foot placement, forward velocity and body orientation of a one-legged hopping robot", *Robotica*, 21, pp. 45-57.

Yoshikawa, T., 1985a, "Manipulability of Robotic Mechanisms", *The international Journal of Robotics Research*, 4(2), pp.3-9.

Yoshikawa, T., 1985b, "Dynamic Manipulability of Robot Manipulators", *Journal of Robotic Systems*, 2(1), pp.113-124.

Zheng, Y.F. and Hemami, H., 1985, "Mathematical modeling of a robot collision with its environment", *Journal of Robotic Systems*, 2(3), pp. 289-307.